

A combinatorial system to examine the enzymatic repair of multiply damaged DNA substrates

Chia Wei Hsu^{1,2,†}, James W. Conrad^{1,†}, Mark L. Sowers^{1,2,*}, Tuvshintugs Baljinnyam¹, Jason L. Herring¹, Linda C. Hackfeld¹, Sandra S. Hatch^{3,4} and Lawrence C. Sowers^{1,5,*}

¹Department of Pharmacology and Toxicology, University of Texas Medical Branch, 301 University Boulevard, Galveston, TX 77555, USA, ²MD-PhD Combined Degree Program, University of Texas Medical Branch, 301 University Boulevard, Galveston, TX 77555, USA, ³Department of Radiation Oncology, University of Texas Medical Branch, 301 University Boulevard, Galveston, TX 77555, USA, ⁴Department of Radiation Oncology, University of Texas MD Anderson Cancer Center, Houston, TX 77030, USA and ⁵Department of Internal Medicine, University of Texas Medical Branch, 301 University Boulevard, Galveston, TX 77555, USA

Received January 20, 2022; Revised May 18, 2022; Editorial Decision June 04, 2022; Accepted June 07, 2022

ABSTRACT

DNA damage drives genetic mutations that underlie the development of cancer in humans. Multiple pathways have been described in mammalian cells which can repair this damage. However, most work to date has focused upon single lesions in DNA. We present here a combinatorial system which allows assembly of duplexes containing single or multiple types of damage by ligating together six oligonucleotides containing damaged or modified bases. The combinatorial system has dual fluorescent labels allowing examination of both strands simultaneously, in order to study interactions or competition between different DNA repair pathways. Using this system, we demonstrate how repair of oxidative damage in one DNA strand can convert a mispaired T:G deamination intermediate into a T:A mutation. We also demonstrate that slow repair of a T:G mispair, relative to a U:G mispair, by the human methyl-binding domain 4 DNA glycosylase provides a competitive advantage to competing repair pathways, and could explain why CpG dinucleotides are hotspots for C to T mutations in human tumors. Data is also presented that suggests repair of closely spaced lesions in opposing strands can be repaired by a combination of short and long-patch base excision repair and simultaneous repair of multiply damage sites can potentially lead to lethal double strand breaks.

INTRODUCTION

The DNA of all living organisms is persistently damaged by endogenous reactive molecules that form an array of dam-

age products including strand breaks as well as base and deoxyribose adducts (1–3). Estimates suggest the magnitude of endogenous damage can exceed tens of thousands of lesions per cell per day. On top of endogenous damage, DNA can also be damaged by exogenous mutagens such as radiation. Chemotherapy agents and radiation can cause complex DNA damage, including inter- and intra-strand cross-links (4–16). If unrepaired, these damaged sites can be lethal to cells. Alternatively, they can miscode during DNA replication, and or repair, resulting in genetic mutations.

In radiation oncology, this is exploited by using high energy radiation to induce single and double-stranded breaks. In addition, a major mechanism of DNA damage is the production of clustered oxidative damage produced by free radicals (13,14). Clustered DNA damage is believed to be a major cause of cell death as the endogenous repair processes involved can induce double strand breaks (13–16).

Within cells, several pathways exist to repair the multitude of distinct forms of DNA damage. Potentially lethal double strand breaks can be repaired by homologous and non-homologous end joining (17–20), bulky DNA lesions can be repaired by nucleotide excision repair (NER) (21–25) while most single-base damage can be repaired by the base excision repair (BER) pathway (26–29). Within these major repair pathways, multiple enzymes and several sub-pathways have also been described. While each major repair pathway targets certain types of DNA damage, there is redundancy among them as well as their sub-pathways. This indicates the potential for competition, cooperation, or collision of different DNA repair pathways.

A substantial number of laboratories have contributed to the development of methods to measure DNA damage, understand the structures of damage sites, and the interactions of damaged sites with DNA polymerases and DNA repair enzymes. Most of this work to date has focused upon sin-

*To whom correspondence should be addressed. Tel: +1 409 772 9678; Email: lasowers@UTMB.edu

†The authors wish it to be known that, in their opinion, the first two authors should be regarded as Joint First Authors.

gle, defined DNA lesions. However, damage events can occur in proximity to one another in either the same DNA strand or in opposing DNA strands (16,30–35). The repair of multiply damaged DNA substrates introduces another level of complexity involving potential competition between distinct DNA repair pathways that could lead to unanticipated biological outcomes.

A focus of our laboratory is on understanding the mechanisms leading to frequent mutations observed in critical genes that drive human tumor development. The mutational landscape of human tumors is dominated by C to T transition mutations, with hotspots occurring at CpG dinucleotides (36–40). The hydrolytic deamination of cytosine to uracil and 5-methylcytosine to thymine are frequently invoked as mechanisms to explain such mutations (41–45). Alternatively, oxidative damage to human tissue is also thought to drive DNA damage and promote tumor development. However, oxidative damage which produces 8-oxoguanine generally induces G to T transversion mutations, not the more common C to T mutations (46–50). A conundrum therefore exists with respect to explaining how oxidative DNA damage might promote C to T transition mutations at CpG sites.

In order to investigate the potential interactions among DNA repair pathways on multiply damaged DNA substrates, we have developed a combinatorial system that allows the construction of DNA duplexes containing single or multiply damaged sites in one or both DNA strands. Oligonucleotides containing fluorophores are ligated with synthetic oligonucleotides containing defined damage to form a 77/79-base duplex corresponding to a region of exon 7 of the p53 gene, a known mutational hotspot (36,51).

With this system, we reconstitute components of the base excision repair (BER) pathway involving glycosylase cleavage of a damaged or mispaired base, cleavage of the abasic site and phosphodiester backbone by lyases, DNA repair synthesis by DNA polymerase β (pol β), and completion of the repair cycle by a DNA ligase. With this system, repair activities on multiply damaged substrates can be followed in both strands simultaneously. We have used this system to study interactions and competition among components of the BER pathway. Our results with this system suggest a possible mechanism by which oxidative DNA damage could drive C to T mutations, and why such mutations occur more frequently at CpG dinucleotides. We also present data in support of a new mechanism for the repair of closely spaced, clustered damage involving a combination of both short and long-patch base excision repair.

MATERIALS AND METHODS

Oligonucleotide synthesis, purification and characterization

Oligonucleotides. A 79 base-long portion of the p53 exon 7 gene containing a mutational hotspot (51) was selected for the system described here (Figure 1). Six oligonucleotides are required to form the full-length duplex. The 5'-end of the 79-bp upper strand is labelled with 6-carboxyfluorescein (FAM) while the 5'-end of the 77-bp lower strand is labelled with sulfo-cyanine5 (Cy5). The two oligonucleotides forming the central duplex can contain modified or damaged bases (X or Z) in either strand and the sequence of

the complementary strand can be modified to generate mismatches (Y). All oligonucleotides were prepared by standard phosphoramidite solid phase methods by Integrated DNA Technologies (IDT), MilliporeSigma, or in house.

Enzymes. Restriction endonucleases (BsrI, cat# R0527S, HaeIII, cat# R0108S, HpaII, cat# R0171S and MspI, cat# R0106S), DNA ligases (T4 DNA ligase, cat# M0202S and *E. coli* DNA ligase, cat# M0205S), Uracil DNA glycosylase (UDG, cat# M0280S), human AP endonuclease 1 (APE1, cat# M0282S), and a thermostable AP endonuclease IV (Tth, cat# M0294S) were purchased from New England Biolabs (NEB).

Human hUNG2 (UNG-1547H) was obtained from Creative BioMart (Shirley, NY). A bifunctional human 8-oxoguanine DNA glycosylase-AP lyase (hOGG1, cat# NBP1-45317-01mg), human DNA polymerase beta (pol β , cat# NBP1-72434-0.5mg) were obtained from Novus Biologicals.

Plasmid DNA (pET28c(+)) encoding full-length human thymine DNA glycosylase (hTDG) (NM_003211.6) with an N-terminal his-tag was obtained from Addgene (cat# 70758). Human thymine DNA glycosylase (hTDG) was expressed as described previously, with the following modifications: bacterial cultures were induced with isopropyl β -D-1-thiogalactopyranoside (0.5 mM) and cultured at 15°C for 22 h (52). The DNA sequence encoding hMBD4 (NM_003925.3) containing an N-terminal his-tag, was inserted into a pET28a(+) vector by Genscript (Piscataway, NJ) (53). hMBD4 was prepared by induction with isopropyl β -D-1-thiogalactopyranoside (0.5 mM) and cultured at 30°C for 6 h. The hybrid thymine DNA glycosylase (hyTDG) was prepared similarly and is described in detail elsewhere (54).

Buffers.

- IDTE™ buffer (IDT, cat# 11-05-01-05) contains 10 mM Tris, 0.1 mM EDTA, pH 7.5
- Thymine DNA glycosylase (TDG) buffer contains 10 mM K_2HPO_4 , 30 mM NaCl, 40 mM KCl, pH 7.7
- T4 ligase reaction buffer contains 50 mM Tris-HCl, 10 mM $MgCl_2$, 1 mM ATP, 10 mM DTT, pH 7.5 (NEB, cat# B0202S)
- Extraction buffer contains 0.3 M sodium acetate, 1 mM EDTA, pH 8.0
- CutSmart™ buffer contains 50 mM potassium acetate, 20 mM Tris-acetate 10 mM magnesium acetate 100 μ g/ml BSA, pH 7.9 (NEB, cat# B7204S)
- NEBuffer™ 3.1 contains 100 mM NaCl, 50 mM Tris-HCl, 10 mM $MgCl_2$, 100 μ g/ml BSA, pH 7.9 (NEB, cat# B7203S)

Assembly, ligation and purification of a multiply damaged substrate. Oligonucleotides were suspended in IDTE buffer at a concentration of 100 μ M based upon oligonucleotide amounts supplied by the manufacturer. Duplexes containing fluorescently labeled oligonucleotides were prepared by mixing labeled strands with a 10% excess of the unlabeled strand followed by heating to 95°C for 2 min and slow cooling. The unlabeled middle duplex was prepared similarly.

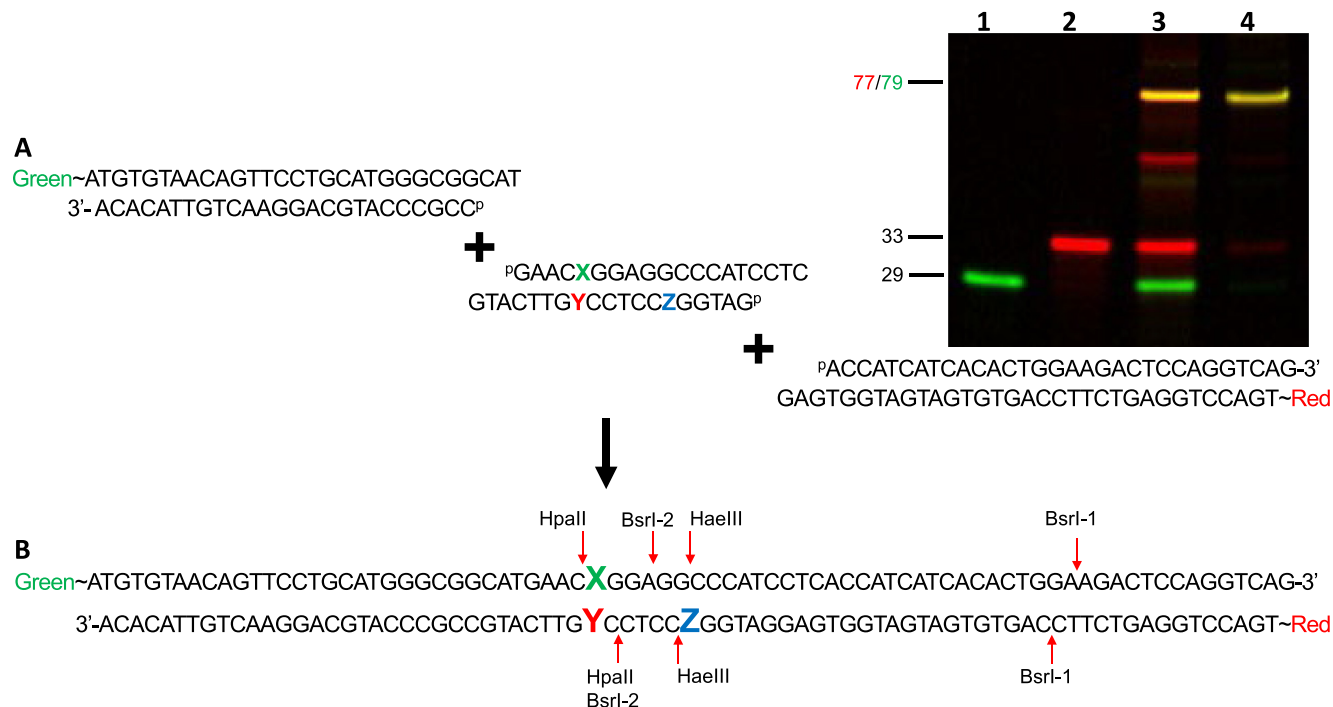


Figure 1. Assembly of a combinatorial system to examine the repair of multiply damaged DNA. (A) Oligo sequences used in the ligation reaction and representative gel showing unligated FAM labeled strand (lane 1), unligated Cy5 labeled strand (lane 2), post ligation reaction products (lane 3), and post gel purification product (lane 4). A superscript 'P' denotes a 5' phosphate. (B) Full length oligo sequence with restriction enzyme cut sites. Sites containing modified or replaced nucleotides are labeled 'X', 'Y', and 'Z.' This convention is used to denote each unique multiply damaged substrate 'X:Y:Z' (e.g. C:G:G) in the supplement. BsrI has two potential cut sites denoted BsrI-1 and BsrI-2. A cut at BsrI-1 produces a 65-base green band while a cut at BsrI-2 produces a 37-base green band and a 15-base red band. HaeIII produces 39 base green and red bands. HpaII produces 33- and 43-base green and red bands, respectively.

Ligation of the strands proceeded in two steps without purification of intermediates (Figure 1). First, the 5'-FAM labeled duplex (400 pmol, 10 μ l) was mixed with an equimolar amount of the unlabeled middle duplex (10 μ l), 10 \times T4 ligase buffer (2.8 μ l) and water (4 μ l). T4 ligase (2 μ l, 800 units) was then added followed by gentle mixing and incubation at 22 $^{\circ}$ C for 30 min followed by cooling to 4 $^{\circ}$ C. An equimolar amount of the 5'-Cy5 labeled duplex (10 μ l, 400 pmol) and 10 \times T4 ligase buffer (1.2 μ l) were then added to the reaction mixture which was incubated at 22 $^{\circ}$ C for 30 min followed by heating at 65 $^{\circ}$ C for 10 min. After cooling, glycerol (10 μ l) was added.

The entire 50 μ l reaction volume was loaded into one well of a 10 cm 15% native polyacrylamide gel and purified using the modified crush and soak method (55). The full-length duplex labeled in both strands was separated from unligated sequences by electrophoresis at 180 V (18 V/cm) for 1 h. The fluorescent gel band corresponding to the full-length duplex was excised from the gel, crushed, and placed into 1 ml of extraction buffer and heated to 95 $^{\circ}$ C for 5 min, frozen to -80 $^{\circ}$ C, followed by thawing at 95 $^{\circ}$ C. The vial containing the extracted duplex was then centrifuged (14 000 \times g, 5 min) and the supernatant is transferred to another vial. The residual in the original vial was extracted a second time with 0.5 ml extraction buffer. Supernatants were combined and the oligonucleotide duplex was concentrated with an Amicon Ultra-0.5 ml, 10 kDa centrifuge filter (Fisher, cat# UFC501096). The concentration of the full-length duplex

was determined by measuring the UV spectrum and using an extinction coefficient of 1 011 122 M $^{-1}$ cm $^{-1}$ (56).

Characterization of the 79-base duplex with restriction endonucleases and DNA glycosylases. The sequences of the full-length oligonucleotides were confirmed by restriction endonuclease cleavage followed by electrophoresis. Restriction sites are shown in Figure 1. Each restriction endonuclease reaction consisted of 2.5 pmol duplex (0.63 μ l), and either CutSmartTM buffer or NEBufferTM 3.1 and 0.5 μ l restriction enzyme (5–10 units). Reactions were incubated at 37 $^{\circ}$ C for 1 h and then an equal volume of formamide was added, followed by heating at 95 $^{\circ}$ C for 10 min. After heating, samples were loaded onto an 8 M urea, 15% polyacrylamide gel, and electrophoresed at 180 V using a 10 cm gel (Bio-Rad Mini-PROTEAN, cat# 1658004). Gels were visualized with a Storm 860 Molecular Imager (Molecular Devices).

The location of modified bases (8-oxoguanine or uracil), or mispaired bases (T:G), were confirmed by incubating 2.5 pmol duplex with a glycosylase in a buffer and at a temperature consistent with that glycosylase. The hyTDG reaction was incubated at 65 $^{\circ}$ C whereas the others (hOGG1, hTDG, UDG) were incubated at 37 $^{\circ}$ C. When monofunctional glycosylases were used, the resulting abasic site was cleaved with either NaOH or Tth lyase. Reactions were quenched by the addition of an equal volume of formamide followed by gel electrophoresis and visualization as described.

Reconstitution of DNA repair reactions. In general, DNA repair reconstitution was performed with 2.5 pmol duplex with CutSmart™ buffer in a final reaction volume of 12.5 μ l. If dNTP's (20 μ M) or NAD⁺ (26 μ M) were included, they were added to the oligonucleotide duplex solution. Enzymes, possibly including a glycosylase (hOGG1, 6.1 pmol; hTDG, 31 pmol; hyTDG 16.8 pmol; UDG 2.5 U), human AP endonuclease (5 U), pol β (6.2 pmol) and a ligase (*E. coli* ligase, 5 U; T4 ligase 200 U) were typically combined and added together to initiate DNA repair, as indicated in each figure. An exception was with hyTDG, which was used to remove T from a T:G mispair. In that case, the reaction was conducted at 65°C with hyTDG, cooled and then the remainder of the components were added. Otherwise, reactions were incubated at 37°C for 1 h. Reactions that were subsequently probed with restriction endonucleases were first heat inactivated at 80°C for 20 min and then cooled. Restriction enzymes were added and incubated for an additional hour at an appropriate temperature. Following addition of an equal volume of formamide and heating at 95°C for 5 min, reaction components were separated by gel electrophoresis and visualized with a Storm imager as described.

Image processing. The Cy5 fluorophore was scanned using normal sensitivity while FAM was scanned using the high sensitivity mode of the Storm imager. Gel files were imported into ImageJ (v1.53e) and background was reduced by adjusting the brightness and contrast, respectively. A composite pseudo colored image was prepared by merging channels. The Cy5 scan is colored red and FAM green, resulting in a yellow band when oligos overlap by convention in ImageJ. Final images were cropped for visualization purposes.

RESULTS AND DISCUSSION

Assembly of a dual color combinatorial repair system

The repair of multiply damaged DNA substrates can involve competition among DNA repair pathways and potentially generate unanticipated biological outcomes. To study this potential complexity, we have constructed a combinatorial system that allows examination of reconstituted DNA repair pathways on multiply damaged substrates and simultaneous observation of both strands of a duplex. We have found that fluorescently labelled oligonucleotides in this system can be measured with sensitivity approaching that of traditional ³²P-end labeling.

The system was constructed with a series of oligonucleotides prepared by standard solid-phase phosphodiester chemistry. Fluorescently labeled oligonucleotides were synthesized independently of sequences containing damaged or modified bases and then combined and ligated to form a longer duplex (Figure 1). The upper FAM-labeled strand (green) is 79 bases in length when ligated, and the lower Cy5 strand (red) is 77 bases in length when ligated. The component oligonucleotides can be assembled efficiently and purified by gel electrophoresis in high yield and are stable for long periods of time as opposed to ³²P-labeled sequences which decay over a short period of time.

While 79-base oligonucleotides could potentially be synthesized directly with multiple modified bases, and fluorescent tags by solid phase methods, the yields of full-length sequences decline substantially with each additional modification. In the system reported here, fluorescently tagged sequences need only be synthesized once. Modified bases can be included in the central sequences where alternative protection/deprotection strategies needed for modified bases can be employed. Libraries of modified oligonucleotides can be synthesized and characterized, and complex, multiply damaged substrates constructed from the collection of modified sequences.

Characterization of a multiply damaged substrate

The 77/79 base duplex system described here was designed to be probed with multiple sequence-specific restriction endonucleases to determine outcomes of different repair pathways. It has two potential BsrI cut sites. One site, BsrI-1, generates a 65-base green band and a 15-base red band (Figure 1B). Additionally, a potential BsrI cut site exists between the HpaII and HaeIII cut sites denoted here as BsrI-2 and can produce a 37-base green band (Figure 1B). Oligonucleotide duplexes containing multiply damaged sites were assembled and characterized with restriction endonucleases and DNA glycosylases (Supplementary Figures S3–S15).

In the first sequence studied 'X', 'Y' and 'Z', as shown in Figure 1B, were T, G and 8-oxoguanine (8oxoG or '8'), respectively (Figure 2). This sequence naming convention is denoted as 'T:G-8' in the supplementary figures. This duplex was incubated with our hyTDG glycosylase, which cleaves T from a T:G mispair, and generated a 33-base green oligonucleotide band (Figure 2). Incubation with hOGG1, which excises 8oxoG, generated a 38-base red oligonucleotide band. The products of repair of the T:G mispair were then be probed with HpaII or BsrI endonucleases. If the T:G mispair was repaired to a C:G base pair, this would have allowed HpaII cleavage. If the T:G mispair was converted into a T:A mutation, this would allow cleavage by BsrI (BsrI-2). In Figure 2, we see only cleavage at BsrI-1. When incubated with HaeIII, the duplex containing the 8oxoG cleaved only the upper green strand (Figure 2). If 8oxoG was repaired to a G, this would allow HaeIII to cleave both strands.

While the impact of multiple damaged bases or mismatches on endonuclease or glycosylase cleavage cannot be predicted always *a priori*, the possible sequences resulting from repair can be easily assembled with the system described here and tested as positive controls. Duplexes containing the possible repair intermediates from the systems studied here, probed with glycosylases and restriction endonucleases, are presented as supplementary information (Supplementary Figure S3–S15). Additionally, the original uncropped images are presented in the supplementary information (Supplementary Figure S16–S32).

Repair by the short-patch base excision repair pathway

The first sequence examined here contained a T:G mispair, simulating the deamination of 5-methylcytosine (5mC) to

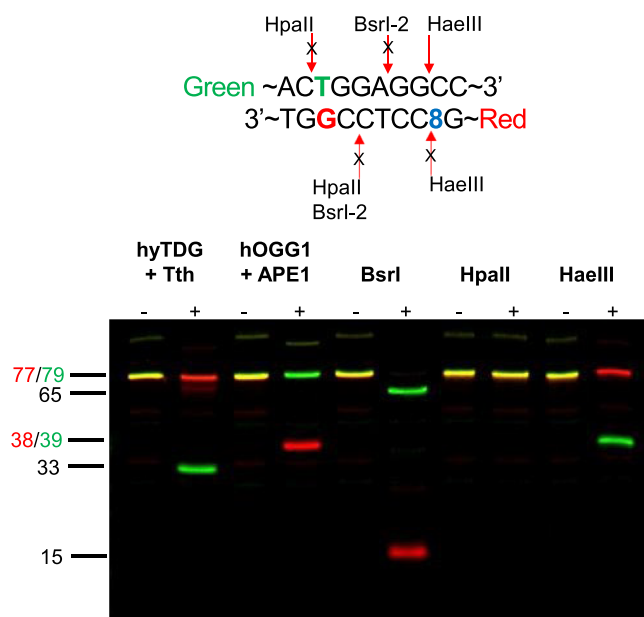


Figure 2. Characterization of a substrate containing complex damage. Glycosylases (hyTDG and hOGG1) or restriction endonucleases (BsrI, HpaII and HaeIII) were tested against a multiply damaged substrate. The T in the upper strand was mismatched with G. An 8-oxoguanine (8') in the lower strand was paired with C. Cleavage by hyTDG and Tth produced a 33-base band, hOGG1 and APE1 a 38-base band, BsrI 65-base and 15-base bands. While HpaII cannot cleave a mismatched duplex, HaeIII was able to cleave the upper strand producing a 39-base band but not the lower strand containing 8-oxoguanine.

T, and an 8-oxoguanine:C base pair, representing oxidative DNA damage (Figure 2). The modified base pairs were separated from one another by five intervening normal base pairs. Repair can be initiated selectively in either strand by incubation with the appropriate glycosylase (Figure 3). Repair of the upper strand can be initiated with hyTDG glycosylase (54) which removes U and T only when mismatched with G (Figure 3A, lane 4). This resulted in 72.4% cleavage. Following base excision, cleavage of the abasic site and cleanup of the 3'-end by APE1 were followed by dCTP and pol β synthesis which generated nicked DNA that was repaired by *E. coli* DNA ligase. The sequential steps in the BER process are shown in lanes 3–7 (Figure 3A). Repair of the upper green strand regenerated the 79-base oligonucleotide (Figure 3A, lane 7). The T:G mismatch has been converted to a C:G base pair as indicated by reconstitution of the HpaII site where 76.8% cleavage was observed (Figure 3A, lane 8).

Repair of the lower strand was initiated by incubation with hOGG1, which was then followed by repair synthesis and ligation, as shown in Figure 3B. In this system, short-patch-BER (SP-BER) was recapitulated by pol β insertion of a single complementary dNTP (dGTP), and inclusion of a ligase (Figure 3B, lane 8). Conversion of the C:8oxoG damage site to a C:G base pair was indicated by cleavage of both upper and lower strands by HaeIII (Figure 3B, lane 8). These results indicate that when repair of both strands was not attempted simultaneously, the repair of either site could proceed independently despite their proximity.

In the system described above, SP-BER was recapitulated. A modified base was removed by a glycosylase, the abasic site cleaved by APE1, and a single base inserted by DNA pol β , followed by completion of the repair cycle by DNA ligase. Alternatively, DNA pol β can insert more than one base by strand-displacement synthesis resulting in the long-patch BER (LP-BER) sub-pathway. In cells, LP-BER would include the FEN-1 endonuclease (57,58), which would cleave the 5'-displaced sequence. Alternatively, the 3'-exonuclease activity of DNA polymerase δ (pol δ) can trim a 3'-overhang followed by ligation (59). In the model system presented here, strand-displacement synthesis was the *in vitro* equivalent of LP-BER.

Repair by strand displacement synthesis and the long-patch BER pathway

We next recapitulated LP-BER by omitting DNA ligase and adding multiple dNTPs (Figure 4). LP-BER was directed to the upper strand by incubation with hyTDG (Figure 4A, lanes 2–4). Addition of dCTP resulted in the insertion of C opposite G (Figure 4A, lane 5), and the incorporation of dGTP, dATP and dTTP allowed strand-displacement synthesis to proceed, regenerating the 79-base upper strand (Figure 4A, lane 8). Conversion of the T:G mismatch to a C:G base pair was verified by predominant HpaII cleavage (Figure 4A, lane 9).

In the repair sequence illustrated in Figure 4A, the 8oxoG in the lower strand remained as no hOGG1 was added. Consequently, incubation of the repaired duplex with HaeIII (Figure 4A, lane 10) resulted in cleavage of the upper green strand, consistent with insertion of C opposite 8oxoG. However, incomplete cutting may have resulted from the minor misincorporation of A opposite 8oxoG. While the oxidized base, 8oxoG, pairs predominantly with C, some misincorporation of A can occur (60). On the other hand, failure of HaeIII to cleave the lower red strand (lane 10) was consistent with the remaining presence of 8oxoG.

LP-BER directed toward the lower strand by incubation with hOGG1, as shown in Figure 4B, revealed a subtle but important event resulting from repair of a multiply damaged DNA duplex. Incubation with hOGG1 generated apparently complete cleavage of the lower red strand (Figure 4B, lane 2). Addition of the other repair components including APE1, pol β and all dNTPs resulted in complete regeneration of the lower red strand (Figure 4B, lanes 3–8). Incubation of the repair products with HaeIII resulted in almost complete cleavage of both strands, indicating removal of 8oxoG and regeneration of the GGCC HaeIII site (Figure 4B, lane 9).

The removal of 8oxoG by hOGG1, followed by strand displacement synthesis, would be expected to insert A opposite the mismatched T in the upper strand. This converted the T:G mismatch into a T:A mutation as illustrated schematically in Supplementary Figure S1. Complete cleavage of the green strand at the BsrI-2 cut site confirmed conversion of the T:G mismatch into a T:A base pair (Figure 4B, lane 10). Deamination of 5mC:G into a T:G mismatch is potentially repairable by BER. However, if LP-BER is initiated from the opposing DNA strand, in the vicinity, the mismatch would be converted into a T:A mutation and no longer recognized

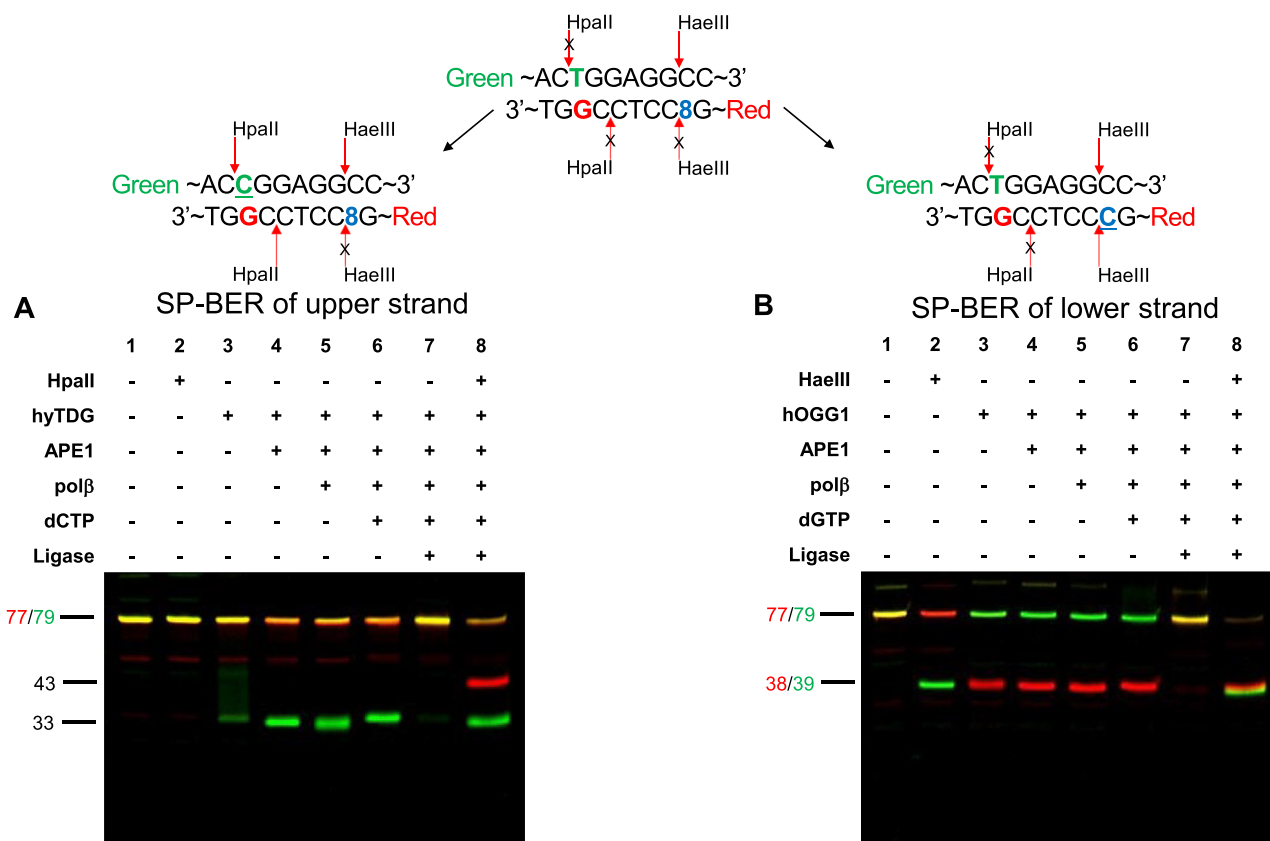


Figure 3. Examination of the repair of the upper and lower strands by the short-patch (SP) BER pathway. Potential restriction endonuclease cleavage sites for repair products are diagrammed at the top for the upper strand (A) or lower strand (B). Nucleotides inserted by pol β are underlined. SP-BER of the upper strand (A) was initiated by hyTDG, and for the lower strand (B) by hOGG1. Cleavage by hyTDG and APE1 produced a 33-base band (A, lane 4) while hOGG1 and APE1 produced a 38-base band (B, lane 4). Restriction endonuclease cleavage of the post-repair products confirmed that the T:G (A) was converted to C:G (HpaII: 43-base and 33-base bands A, lane 8) and the 8-oxoguanine (*8):C was repaired to C:G (HaeIII: 39-base bands B, lane 8).

and/or repaired by the BER pathway. This result establishes that the biological outcome of repair of multiply damaged duplexes can be problematic.

To demonstrate the range of questions that can be addressed with this system, we changed the configuration of the multiple damaged sites by placing the 8oxoG in the upper strand as shown in Figure 5. In this configuration, hOGG1 removes the 8oxoG and initiates repair of the upper strand. Repair synthesis by pol β results in the replacement of the T in the upper strand by C. Comparison of lanes 1 and 10 shows that the CCGG HpaII site has been reconstituted by this repair pathway. The biological significance of this result is that the initiation of the BER pathway in the vicinity of CpG sites could result in demethylation and epigenetic changes. Grin and Ishchenko recently showed that the removal of 5-hydroxymethyluracil by the BER pathway could similarly act as an active demethylation pathway (34).

Competition between short-patch and long-patch repair pathways occurs on the same strand

Potential competition for repair by the short-patch and long-patch pathways in the lower strand was examined next. The duplex described in Figure 4 was probed first with a mixture of hOGG1, APE1, pol β, dGTP and *E. coli*

DNA ligase, simulating SP-BER (Figure 6, lane 2). To simulate LP-BER, ligase was omitted and multiple dNTPs were added (Figure 6, lane 3). In both cases, the 8oxoG was removed, and full-length strands were regenerated. Competition between SP and LP-BER was then initiated by simultaneously adding all components including multiple dNTPs and ligase. As expected, full-length oligonucleotides were generated (Figure 6, lane 4).

In the system studied here, SP-BER of the 8oxoG would leave the T:G mismatch intact. In contrast strand displacement synthesis by LP-BER could replace the G of the T:G mismatch with an A, resulting in a mutation. When the repair product of the SP-BER control was probed with hyTDG (Figure 6, lane 5), the upper green oligo was cleaved as anticipated. In contrast, when the product of LP-BER repair was probed with hyTDG, the product was not cleaved, indicating replacement of the G of the T:G mismatch with A (Figure 6, lane 6). When the product of repair in the presence of all SP and LP components was probed, the green strand was cleaved indicating predominant repair by SP-BER (Figure 6, lane 7). However, hyTDG did not cleave all the product oligonucleotides and therefore some LP-BER may have occurred.

In order to measure the relative amounts of SP and LP-BER, the products of repair were probed with BsrI as shown

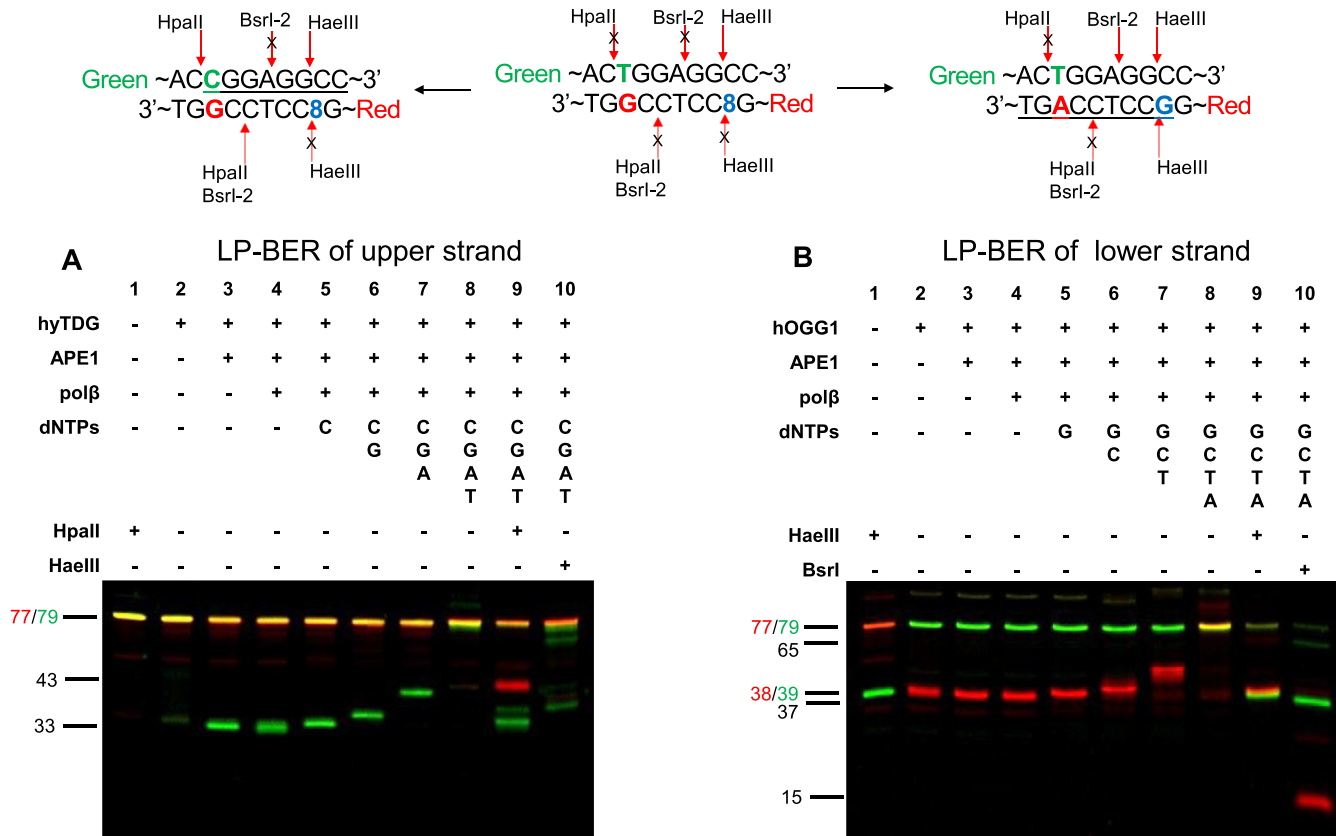


Figure 4. Examination of DNA repair by strand displacement synthesis and the long-patch (LP) BER pathway. The multiply damaged substrate and potential restriction endonuclease cut sites are shown with the top middle oligonucleotide. Repair was initiated in the upper strand by hyTDG (A, lane 3) or in the lower strand by hOGG1 (B, lane 3). Following repair, substrates were probed with restriction endonucleases. Cleavage by HpaII (A, lane 9) confirmed that the T:G mismatch was converted to C:G. Cleavage by HaeII (B, lane 9) confirmed that the 8oxoG:C was repaired to G:C.

in Figure 6, lanes 8–10. SP-BER would leave the T:G mismatch intact, and so the product oligonucleotides would generate only 65- and 15-base long oligonucleotide fragments, corresponding to the BsrI-1 cut site only (Figure 6, lane 8). In contrast, the replacement of the G of the T:G mismatch with A by LP-BER, followed by BsrI, would generate a 37-base long green oligonucleotide (Figure 6, lane 9). If both SP and LP-BER occur, BsrI would generate both 65 (SP) and 37-base (LP) green bands. As shown in Figure 6, lane 10, both green bands were observed. The SP-BER band is 2.5 times the intensity of the LP-BER band indicating that, under the conditions of this experiment, repair by both pathways could occur.

Competition between repair of upper and lower strands by strand displacement synthesis can cause double strand breaks

Repairable damage could potentially occur simultaneously in both strands of a DNA duplex. A hypothetical system is shown in Figure 7A, in which the upper strand has a U:G mismatch, which could result from cytosine deamination, and the lower strand contains an 8oxoG. If both strands were repaired simultaneously by LP-BER, a blunt-end double-strand break could be generated.

In Figure 7B, initiation of repair with hOGG1 resulted in cleavage of the lower strand (Figure 7B, lane 2), and subsequent addition of UDG resulted in cleavage of the upper strand as well (Figure 7B, lane 3). Addition of pol β and dNTPs resulted in the elongation of both the cleaved upper and lower strands. However, extension could only continue until pol β encountered the repair gap in the opposing strand (Figure 7B, lanes 4–8). Blunt-end double strand breaks such as this could be lethal *in vivo*.

The above experiment was repeated, except UDG was replaced with the less efficient hTDG (Figure 7C). As above, the addition of hOGG1 resulted in complete cleavage of the lower strand (Figure 7C, lane 2). In contrast, subsequent addition of hTDG did not cleave all the U-containing strand (Figure 7C, lane 3). Repair synthesis by pol β in the presence of dNTPs resulted in elongation of some strands and complete repair of a fraction of the the 8oxoG-containing lower strand (Figure 7C, lane 8). In this case, complete repair of the lower strand could occur because the initiation of repair by hOGG1 was faster than hTDG. This allowed repair of the lower strand before repair of the upper strand was initiated. The outcome of repair in duplexes containing damage in both strands is therefore dependent upon the

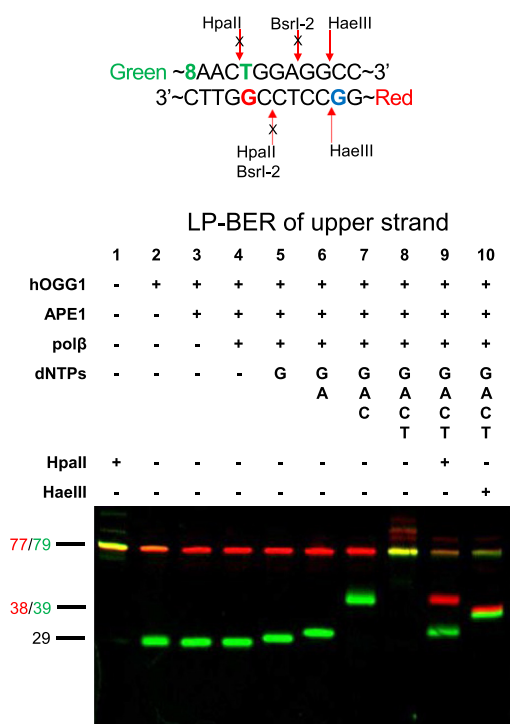


Figure 5. LP-BER repair of 8oxoG can result in demethylation of nearby CpG sites. In the configuration shown above, 8oxoG (‘8’) is on the 5’ side of a T:G mismatch, which could arise from the deamination of 5mC. The BER pathway was initiated by the removal of 8oxoG (‘8’) by hOGG1 (lane 2). Repair synthesis by pol β resulted in the insertion of G (lane 5), the replacement of the mispaired T with C (lane 7), and completion of the repair of the upper strand (lane 8). The CCGG HpaII site was initially blocked by the presence of the T:G mismatch. However, after repair synthesis, the T:G was converted to C:G which allowed HpaII cleavage (lane 9). This result showed that BER can also function as an active demethylation pathway.

relative activities of the glycosylases that can initiate the repair.

Slow repair of a T:G mismatch alters repair outcome of competition

In the study described above, UDG and hTDG were used to remove U, in competition with the removal of 8oxoG by hOGG1. However, not all glycosylases are as efficient. In the next study, we examined the repair of U:G and T:G with hMBD4, in competition with hOGG1. hMBD4 has two domains: a glycosylase domain and a methyl-binding domain (53,61,62). The methyl-binding domain (MBD) preferentially binds to methylated CpG sites (63). Previous studies have shown hMBD4 glycosylase kinetics to be complicated due to potential competition between the glycosylase and MBD domains (61,64,65).

In Figure 8A, incubation with hMBD4 (15 pmol) and APE1 resulted in the cleavage of ~57% of the U-containing strand. Addition of hOGG1 (12 pmol) resulted in nearly complete cleavage of the lower strand (lane 3). Addition of pol β and dNTPs allowed strand-displacement synthesis to regenerate the full length sequence (lane 6) which was cleaved by BsrI (lane 7). This indicated that in most of the duplexes, U:G was converted to U:A due to strand displacement synthesis and LP-BER of the lower strand.

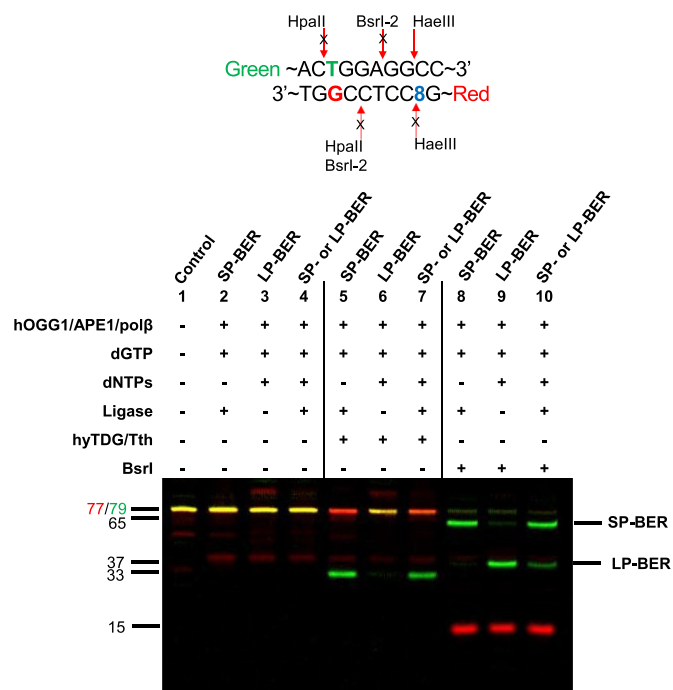


Figure 6. Competition between short-patch (SP-BER) and long-patch (LP-BER) repair can occur on the lower strand. dNTPs denotes an equimolar amount of dCTP, dGTP, dATP and dTTP. Repair of the 8-oxoguanine (‘8’) in the lower strand by SP- or LP-BER pathways with restoration of the full-length sequence was demonstrated in lanes 2 to 4. Post-repair products were examined in lanes 5-7 with hyTDG. The SP-BER repair of the 8oxoG in the lower strand did not alter the T:G mismatch, which was confirmed by hyTDG cleavage (lane 5). However, LP-BER of the 8oxoG in the lower strand converted the T:G mismatch into a T:A base pair, which was not cleaved by hyTDG (lane 6). Competition between SP and LP-BER (lane 7) revealed predominant cleavage with hyTDG, indicating repair occurred mostly by SP-BER. However, hyTDG cleavage cannot reveal low levels of any LP-BER product. Post-repair products were also probed with BsrI (lanes 8-10). Cleavage of the SP-product with BsrI generated a 65-base green band, whereas the LP-product generated a 37-base band. BsrI cleavage of the products of the competition reaction revealed two bands, both SP- and LP-BER, with SP-BER occurring 2.5 times more than LP-BER.

In Figure 8B, the U has been replaced with T generating a T:G mismatch. We observed substantially lower cleavage at this site (~9%, Figure 8B lane 2). In accord with this observation, previous studies have shown hMBD4 to excise U more rapidly than T (61,62,65). The 8oxoG in the opposing strand is efficiently cleaved by hOGG1. Addition of pol β and dNTPs allows strand displacement synthesis (lane 6). Cleavage with BsrI indicated that the T:G mismatch was converted predominantly to a T:A base pair.

Previously, Jones and coworkers (66) measured the excision capacity of extracts from human colon cancer cells for U:G to be substantially greater than the repair of T:G mismatches. The difference in the repair capacity of U:G versus T:G was proposed to explain why C to T mutations at CpG dinucleotides, which are predominantly methylated, appear as mutational hotspots. This study is in accord with those findings. The sluggish repair of T:G relative to the repair of other DNA damage products, would promote the conversion of T:G to T:A which could no longer be repaired. This could be an Achilles’ heel of the human genome.

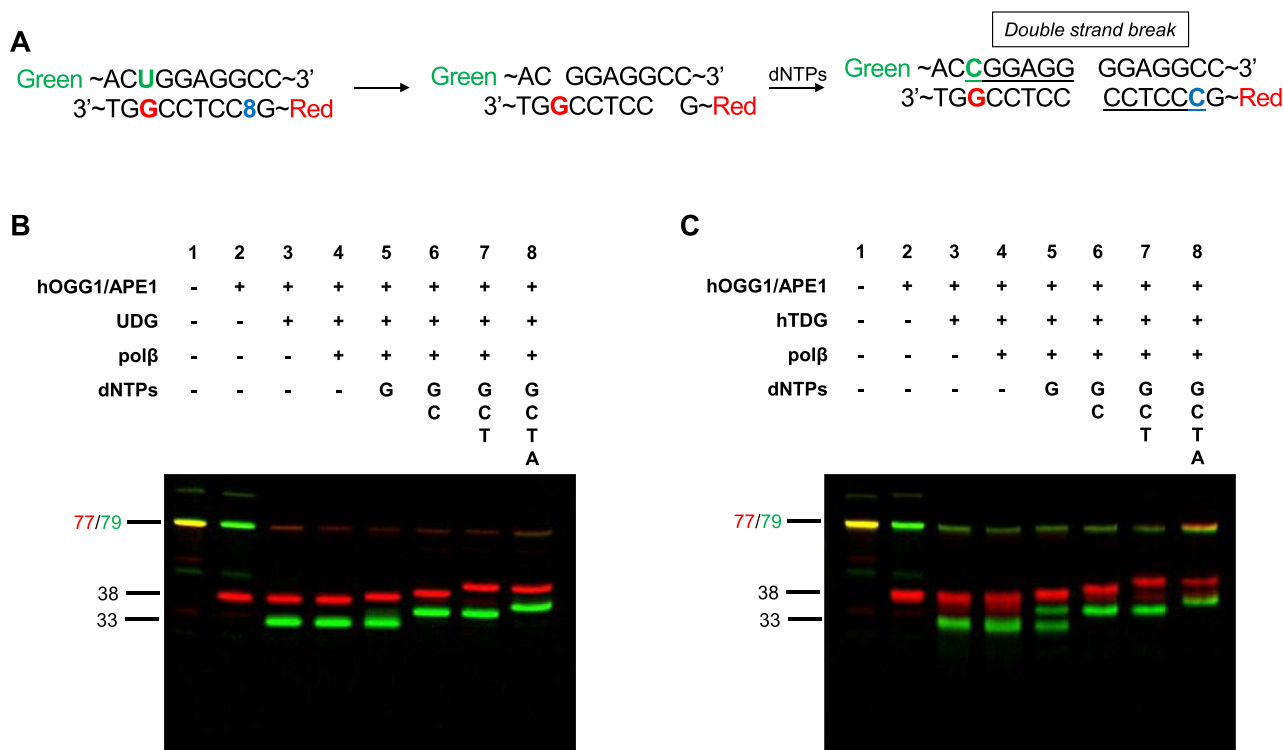


Figure 7. Competition between long-patch repair (LP-BER) of upper and lower strands can lead to a double strand break. (A) Diagram of LP-BER initiated on both strands resulting in double strand breaks with underlined nucleotides inserted by pol β. (B) Repair of both strands was initiated with hOGG1 and UDG. (C) Repair with hOGG1 and the relatively slow enzyme hTDG. Cleavage by UDG or hTDG and APE1 produced a 33-base band while hOGG1 and APE1 produced a 38-base band.

Competition between SP and LP-BER in both upper and lower strands simultaneously

We next examined competition between SP and LP-BER in both strands of a duplex containing a U:G mismatch and an 8oxoG. Simultaneously, glycosylases, APE1, pol β, and dNTPs were added along with the NAD⁺ dependent *E. coli* DNA ligase (Figure 9). As shown in Figure 9A, lane 3, simultaneous addition of both UDG, hOGG1 and APE1 results in removal of uracil (upper strand) and 8-oxoguanine (lower strand) and cleavage of both red and green strands. In Figure 9A, lane 5, repair synthesis was initiated by addition of dGTP only, which allowed SP-BER of the lower red strand and complete restoration of the red strand.

Addition of both dGTP and dCTP, however, created a competition between the repair of the upper and lower strands, allowing approximately half of each strand to be completely repaired by SP-BER (Figure 9A, lane 6). Further, addition of dTTP and dATP allowed strand displacement synthesis to continue; but, extension of each strand appeared to halt when pol β approached the repair site in the opposing strand (Figure 9A, lanes 7 and 8).

Examination of Figure 9A, lane 5 reveals that SP-BER can occur in one strand independently if the opposing lesion cannot be ligated, because the necessary dNTP is absent. When the missing dNTP was restored, SP-BER could occur in both strands but only partially (lane 6). It appears that when repair is attempted simultaneously, the repair of one strand can block complete repair of the other.

The experiment described in Figure 9A was repeated, but UDG was replaced by the less active hTDG (Figure 9B). In contrast, repair was not initiated by hTDG in all green strands and a fraction of them remained intact, serving as a template for repair of the lower red strand (Figure 9B, lane 3). The addition of dGTP allowed for G insertion and potential completion of repair by DNA ligase (Figure 9B, lane 5). The primary difference between the two experiments (Figure 9A versus B) is that SP-BER of the lower red strand appears to be complete when repair is initiated by UDG (Figure 9A, lane 5), but incomplete when hTDG is used in place of UDG. Although the glycosylase activity of hTDG is slower than that of UDG, hTDG also binds tightly to its substrate (67). This could perhaps interfere with ligation of the opposing strand. In Figure 9C and D, the experiment described above was repeated with the ATP-dependent T4 ligase in place of the *E. coli* ligase. Very similar results were obtained.

The data presented in Figure 9 reveals that the repair of DNA damage in one strand of a duplex containing damage in both strands can be inhibited by the presence of repair proteins in the opposing strand. To account for this finding, a model is proposed in Supplementary Figure S2. In this model, a DNA ligase could engage a nicked repair intermediate in either the upper (Supplementary Figure S2C) or lower strand (Supplementary Figure S2D). The presence of a ligase, or glycosylase, in one strand may sterically block the binding of another ligase in the opposing strand. The footprint of *E. coli* ligase is approximately 9 bases on each

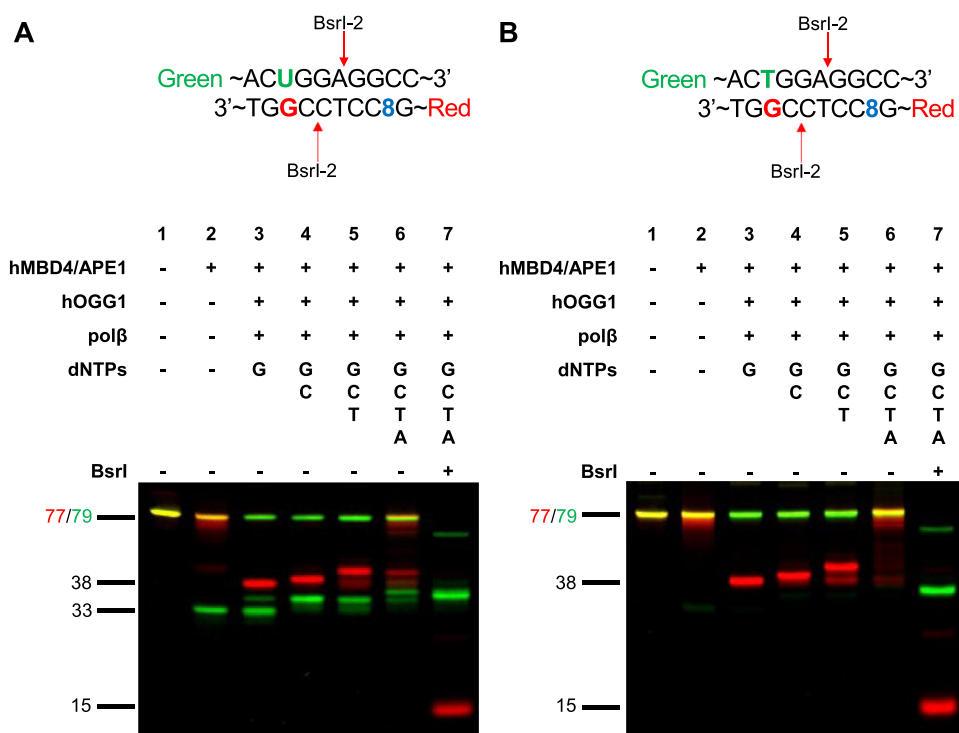


Figure 8. Slow repair of a T:G mismatch alters repair outcome of LP-BER competition. Competition between U and 8oxoG repair is shown in (A) whereas competition between T and 8oxoG is shown in (B). When repair was initiated with hMBD4 and hOGG1 (A, lane 3), the U-containing strand was partially cleaved, whereas the 8oxoG-containing strand was completely cleaved. Subsequent repair with pol β and all dNTPs resulted in predominant repair of both strands with some double strand breaks (A, lane 6). The excision of T:G by hMBD4 (B, lane 2) was much slower than U (A, lane 2). Subsequent repair with pol β and dNTPs generated full length sequences (B, lane 6). BsrI cleavage (A, lane 7) indicated conversion of the U:G to U:A or T:A, whereas in B, lane 7, the predominant repair product was T:A. Panel B revealed that most of the 8oxoG-containing strand was repaired before hMBD4 could initiate repair of the T:G mismatch.

side of the nick, leaving a gap or nick in the opposing strand within its footprint (68).

The data presented here suggests an additional complexity of repairing nearby damage in opposing strands. Two closely spaced nicks in opposing DNA strands, for example arising from restriction endonuclease cleavage, could be ligated sequentially in one strand and then the other. However, our results suggest that a DNA ligase engaged in one strand can hinder the binding of a ligase to the opposing strand. Surprisingly, even though a ligase is engaged to a nicked template, it appears that pol β can insert more than one nucleotide. If more than one nucleotide is added, the repair gap in the strand opposite the ligase can no longer be ligated, likely explaining truncation of half of the strands even in the presence of a DNA ligase.

In cells, the repair of DNA junctions with either 5'- or 3'-overhangs could be resolved by either FEN1 nuclease or the 3'-exonuclease activity of pol δ, followed by ligation (59). The repair pathway described here could provide a previously unrecognized mechanism for the repair of closely spaced damaged in opposing DNA strands.

Competition for the repair of a multiply damaged substrate by all human enzymes

In the last experiment, the system containing a U:G mismatch and 8oxoG was repaired by all human enzymes (Fig-

ure 10). SP-BER was first examined in one strand at a time. When the substrate was incubated with hUNG2, complete cleavage of the green strand was observed (lane 2). Addition of dCTP, pol β and hLIGIII/XRCC1 allowed ~60% completion of SP-BER (lane 3). Initiation of repair in the opposing strand with hOGG1 led to cleavage of most of the red lower strand (lane 4). Addition of dGTP, pol β and hLIGIII/XRCC1 led to approximately 57% SP-BER (lane 5).

When SP-BER was initiated simultaneously in the upper and lower strands, both strands were cleaved. Unexpectedly, the addition of pol β, dNTPs and hLIGIII/XRCC1 did not allow completion of SP-BER in either strand (lane 7). Both strands were elongated a few bases by pol β, but no ligation occurred. We observed SP-BER with either damage product in either strand, when done independently (lanes 3 and 5). However when repair is done simultaneously, in close proximity using all human enzymes, the outcome is a potentially lethal double-strand break.

SUMMARY AND CONCLUSIONS

We have established a combinatorial system to monitor DNA repair in the presence of multiple DNA lesions. This system has several advantages over traditional ³²P-end labelled systems, particularly the capacity to monitor the repair of both strands simultaneously. With this system, we

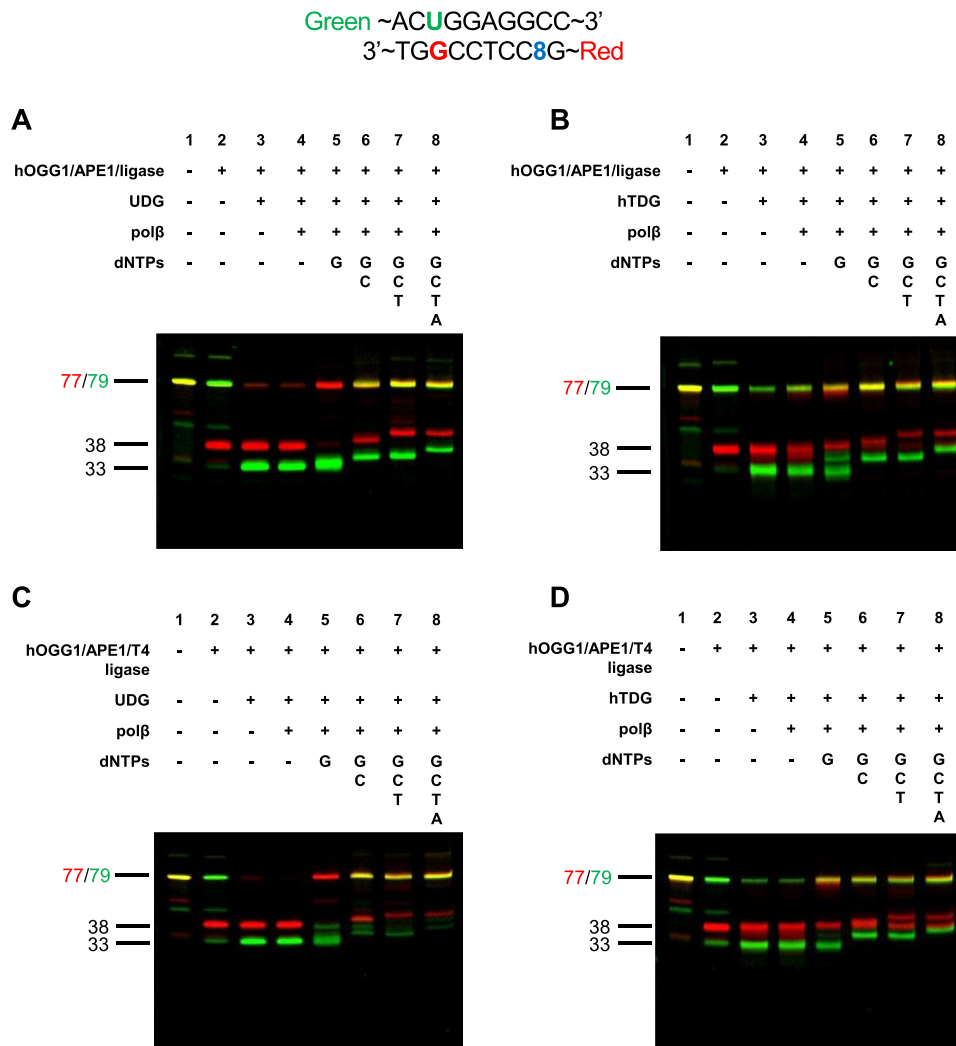


Figure 9. Competition between SP-BER and LP-BER simultaneously in both upper and lower strands is compared with different combinations of repair enzymes. Competition between UDG and hOGG1 is shown in panels A and C, and between hTDG and hOGG1 in panels B and D. In panel A and B, SP-BER was completed by *E. coli* ligase, whereas in panels C and D, T4 ligase was used. In panel A, both strands were completely cleaved by UDG and hOGG1. Addition of pol β and dGTP allowed complete repair of the lower strand (A, lane 5). Interestingly, simultaneous addition of dGTP and dCTP resulted in less repair of the lower strand and significant amounts of truncated strands (A, lane 8). Replacement of UDG with hTDG allowed preferential repair of the lower strand. Similar results were obtained when *E. coli* ligase was replaced with T4 ligase (C&D).

have demonstrated a subtle, but important aspect of competition between different repair pathways. Specifically, LP-BER initiated in one strand can convert a nearby mismatched intermediate into a mutation. As shown here, once a T:G mismatch has been converted to a T:A mutation, it can no longer be recognized and repaired. The C:G to T:A mutation recapitulated in this model system is a hotspot in the human p53 gene in many human tumors (48). The repair-competition model presented here may therefore explain how increased oxidative damage to DNA could contribute to increased C to T mutations, particularly if the sugar fragment becomes damaged.

Factors that influence repair path choice, particularly between SP and LP-BER are not well understood. Defining these factors will be important in understanding the biological consequences of multiply damaged DNA substrates.

Within this context, it is interesting that an additional but little studied property of the adenomatous polyposis coli (APC) protein is to interact with a DNA repair complex and inhibit LP-BER (69). APC is frequently mutated in human cancers, and its loss could allow increased LP-BER conversion of deaminated mismatches to T:A mutations as demonstrated here.

The mutations observed in human tumors include an abundance of C to T mutations at CpG dinucleotides, likely due to cytosine methylation at CpG. Slow repair of T:G, arising from 5mC deamination has been known for some time and is an important contributor to the hotspot frequency of C to T mutations at CpG (66). When viewed within the context of multiply damaged substrates and potentially competing DNA repair pathways as described here, slow repair of T:G could lead to preferential repair

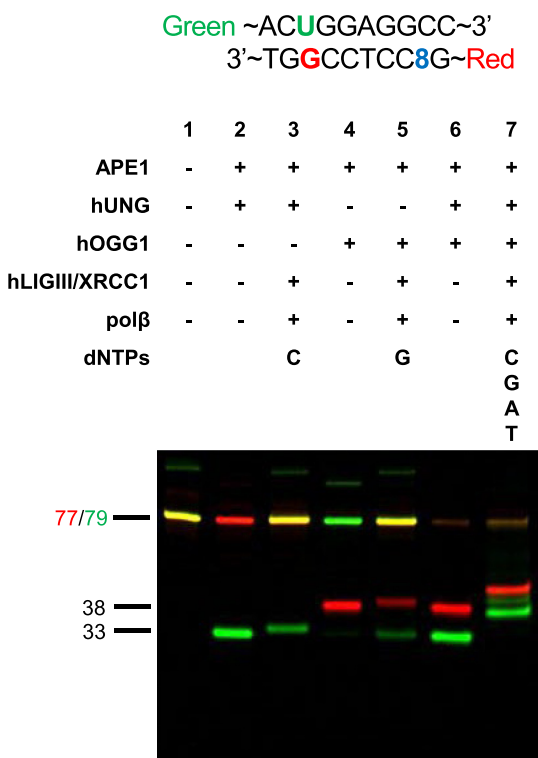


Figure 10. Competition for repair of a multiply damaged substrate using all human enzymes results in a double-strand break. In the system shown above, repair was initiated first on the upper strand by incubation with hUNG2 (lane 2). Addition of pol β , dCTP and hLIGIII/XRCC1 resulted in 60% completion of repair by the SP-BER pathway (lane 3). Repair was then initiated on the lower strand by incubation with hOGG1 (lane 4) which removed the 8oxoG ('8'). Addition of pol β , dGTP and hLIGIII/XRCC1 allowed the completion of repair (57%) by SP-BER. When repair was initiated on both upper and lower strands simultaneously, both strands were cleaved. Addition of pol β , dNTPs and hLIGIII/XRCC1 resulted in partial elongation of both strands, with no ligation. This is in contrast to the data presented with *E. coli* ligase and T4 ligase shown in Figure 9.

of other sites, possibly resulting in the conversion of a T:G intermediate to an irreparable T:A mutation. Understanding the interactions among DNA repair pathways, particularly on multiply damaged substrates may provide new important insights into mechanisms that underlie the development of human tumors (11,70).

Limitations of this approach

The model system described here allows for the construction of complex DNA damage in multiple configurations. The purpose of this work was to develop a tool to study the repair of complex DNA damage. We used this tool to ask 'what if' questions about potential repair pathways and their competition. Labeling both strands allowed repair events to be followed on both strands simultaneously. The systems studied here have revealed some unanticipated results. However, other factors present within cells could enhance or diminish some of the pathways examined here and alter the outcome of competition among repair pathways. In this initial study, only a fraction of known repair enzymes were included.

SUPPLEMENTARY DATA

Supplementary Data are available at NAR Online.

FUNDING

NIH NCI [R01CA228085, in part]; John Sealy Distinguished chair in Cancer Biology; John Sealy Distinguished Centennial Chair in Radiation Therapy; NSF [EFRI1933321]; C.W.H. and M.L.S. were supported in part by the UTMB physician-scientist training program; C.W.H. was supported in part by NIH [F30 CA225116]. Funding for open access charge: NIH; NSF; University of Texas Medical Branch at Galveston.

Conflict of interest statement. None declared.

REFERENCES

- Mullaart,E., Lohman,P.H.M., Berends,F. and Vijg,J. (1990) DNA damage metabolism and aging. *Mutat. Res.*, **237**, 189–210.
- Lindahl,T. (1993) Instability and decay of the primary structure of DNA. *Nature*, **362**, 709–715.
- Tubbs,A. and Nussenzweig,A. (2017) Endogenous DNA damage as a source of genomic instability in cancer. *Cell*, **168**, 644–656.
- Geacintov,N.E. and Swenberg,C.E. (1991) Chemical, molecular biology, and genetic techniques for correlating DNA base damage induced by ionizing radiation with biological end points. *Basic Life Sci.*, **58**, 453–474.
- Guengerich,F.P., Kim,M.-S., Müller,M. and Lowe,L.G. (1997) Chemical mechanisms of formation of DNA-Carcinogen adducts, elucidation of potential of adducts for mutagenicity, and mechanisms of polymerase fidelity and mutation in the presence of adducts. In: Müller-Hermelink,H.K., Neumann,H.-G. and Dekant,W. (eds). *Risk and Progression Factors in Carcinogenesis*. Springer Berlin Heidelberg, Berlin, Heidelberg, pp. 49–63.
- Hoeijmakers,J.H.J. (2001) The consequences of DNA injury genome maintenance mechanisms for preventing cancer. *Nature*, **411**, 366–374.
- Gates,K.S. (2009) An overview of chemical processes that damage cellular DNA: spontaneous hydrolysis, alkylation, and reactions with radicals. *Chem. Res. Toxicol.*, **22**, 1747–1760.
- Lonkar,P. and Dedon,P.C. (2011) Reactive species and DNA damage in chronic inflammation: reconciling chemical mechanisms and biological fates. *Int. J. Cancer*, **128**, 1999–2009.
- Nejad,M.I., Johnson,K.M., Price,N.E. and Gates,K.S. (2016) A new cross-link for an old cross-linking drug: the nitrogen mustard anticancer agent mechlorethamine generates cross-links derived from abasic sites in addition to the expected drug-bridged cross-links. *Biochemistry*, **55**, 7033–7041.
- Cadet,J., Davies,K.J.A., Medeiros,M.H., Di Mascio,P. and Wagner,J.R. (2017) Formation and repair of oxidatively generated damage in cellular DNA. *Free Radic. Biol. Med.*, **107**, 13–34.
- Hsu,C.W., Sowers,M.L., Hsu,W., Eyzaguirre,E., Qiu,S., Chao,C., Mouton,C.P., Fofanov,Y., Singh,P., Sowers,L.C. *et al.* (2017) How does inflammation drive mutagenesis in colorectal cancer? *Trends Cancer Res.*, **12**, 111–132.
- Kay,J., Thadhani,E., Samson,L. and Engelward,B. (2019) Inflammation-induced DNA damage, mutations and cancer. *DNA Repair (Amst.)*, **83**, 102673.
- Ward,J.F. (1981) Some biochemical consequences of the spatial distribution of ionizing radiation-produced free radicals. *Radiat. Res.*, **86**, 185–195.
- Sage,E. and Shikazono,N. (2017) Radiation-induced clustered DNA lesions: repair and mutagenesis. *Free Radic. Biol. Med.*, **107**, 125–135.
- Blaisdell,J.O. and Wallace,S.S. (2001) Abortive base-excision repair of radiation-induced clustered DNA lesions in escherichia coli. *Proc. Natl. Acad. Sci. U.S.A.*, **98**, 7426–7430.
- D'souza,D.I. and Harrison,L. (2003) Repair of clustered uracil DNA damages in escherichia coli. *Nucleic Acids Res.*, **31**, 4573–4581.
- Lieber,M.R. (2010) The mechanism of double-strand DNA break repair by the nonhomologous DNA end-joining pathway. *Annu. Rev. Biochem.*, **79**, 181–211.

18. Daley, J.M., Niu, H., Miller, A.S. and Sung, P. (2015) Biochemical mechanism of DSB end resection and its regulation. *DNA Repair (Amst.)*, **32**, 66–74.
19. Wright, W.D., Shah, S.S. and Heyer, W.D. (2018) Homologous recombination and the repair of DNA double-strand breaks. *J. Biol. Chem.*, **293**, 10524–10535.
20. Sallmyr, A. and Tomkinson, A.E. (2018) Repair of DNA double-strand breaks by mammalian alternative end-joining pathways. *J. Biol. Chem.*, **293**, 10536–10549.
21. Lehmann, A.R. (2011) DNA polymerases and repair synthesis in NER in human cells. *DNA Repair (Amst.)*, **10**, 730–733.
22. Marteiijn, J.A., Lans, H., Vermeulen, W. and Hoeijmakers, J.H.J. (2014) Understanding nucleotide excision repair and its roles in cancer and ageing. *Nat. Rev. Mol. Cell Biol.*, **15**, 465–481.
23. Spivak, G. (2016) Transcription-coupled repair: an update. *Arch. Toxicol.*, **90**, 2583–2594.
24. Kumar, N., Raja, S. and Van Houten, B. (2020) The involvement of nucleotide excision repair proteins in the removal of oxidative DNA damage. *Nucleic Acids Res.*, **48**, 11227–11243.
25. Shafirovich, V. and Geacintov, N.E. (2021) Excision of oxidatively generated guanine lesions by competitive dna repair pathways. *Int. J. Mol. Sci.*, **22**, 2698.
26. Lindahl, T. (2001) Keynote: past, present, and future aspects of base excision repair. In: *Base Excision Repair, Progress in Nucleic Acid Research and Molecular Biology*. Academic Press, Vol. **68**, pp. xvii–xxx.
27. Wilson, S.H. and Kunkel, T.A. (2000) Passing the baton in base excision repair. *Nat. Struct. Biol.*, **7**, 176–178.
28. Baiken, Y., Kanayeva, D., Taipakova, S., Groisman, R., Ishchenko, A.A., Begimbetova, D., Matkarimov, B. and Saparbaev, M. (2021) Role of base excision repair pathway in the processing of complex DNA damage generated by oxidative stress and anticancer drugs. *Front. Cell Dev. Biol.*, **8**, 617884.
29. Bhakat, K.K., Sengupta, S. and Mitra, S. (2020) Fine-tuning of DNA base excision/strand break repair via acetylation. *DNA Repair (Amst.)*, **93**, 102931.
30. Dianov, G.L., Timehenko, T.V., Sinitsina, O.I., Kuzminov, A.V., Medvedev, O.A. and Salganik, R.I. (1991) Repair of uracil residues closely spaced on the opposite strands of plasmid DNA results in double-strand break and deletion formation. *MGGmol. Gen. Genet.*, **225**, 448–452.
31. Éot-Houllier, G., Goner, M., Gasparutto, D., Giustranti, C. and Sage, E. (2007) Interplay between DNA N-glycosylases/AP lyases at multiply damaged sites and biological consequences. *Nucleic Acids Res.*, **35**, 3355–3366.
32. Paap, B., Wilson, D.M. and Sutherland, B.M. (2008) Human abasic endonuclease action on multilesion abasic clusters: implications for radiation-induced biological damage. *Nucleic Acids Res.*, **36**, 2717–2727.
33. Sage, E. and Harrison, L. (2011) Clustered DNA lesion repair in eukaryotes: relevance to mutagenesis and cell survival. *Mutat. Res. - Fundam. Mol. Mech. Mutagen.*, **711**, 123–133.
34. Grin, I. and Ishchenko, A.A. (2016) An interplay of the base excision repair and mismatch repair pathways in active DNA demethylation. *Nucleic Acids Res.*, **44**, 3713–3727.
35. Bukowska, B. and Karwowski, B.T. (2018) The clustered DNA lesions – types, pathways of repair and relevance to human health. *Curr. Med. Chem.*, **25**, 2722–2735.
36. Greenblatt, M.S., Bennett, W.P., Harris, C.C. and Hollstein, M. (1994) Mutations in the p53 tumor suppressor gene: clues to cancer etiology and molecular pathogenesis. *Cancer Res.*, **54**, 4855–4878.
37. Magewu, A.N. and Jones, P.A. (1994) Ubiquitous and tenacious methylation of the CpG site in codon 248 of the p53 gene may explain its frequent appearance as a mutational hot spot in human cancer. *Mol. Cell Biol.*, **14**, 4225–4232.
38. Tornaletti, S. and Pfeifer, G.P. (1995) Complete and tissue-independent methylation of CpG sites in the p53 gene: implications for mutations in human cancers. *Oncogene*, **10**, 1493–1499.
39. Iengar, P. (2012) An analysis of substitution, deletion and insertion mutations in cancer genes. *Nucleic Acids Res.*, **40**, 6401–6413.
40. Poulos, R.C., Olivier, J. and Wong, J.W.H. (2017) The interaction between cytosine methylation and processes of DNA replication and repair shape the mutational landscape of cancer genomes. *Nucleic Acids Res.*, **45**, 7786–7795.
41. Lindahl, T. and Nyberg, B. (1974) Heat-induced deamination of cytosine residues in DNA. *Biochemistry*, **13**, 3405–3410.
42. Sowers, L.C., Sedwick, W.D., Shaw, B.R., David Sedwick, W. and Shaw, B.R. (1989) Hydrolysis of N3-methyl-2'-deoxycytidine: model compound for reactivity of protonated cytosine residues in DNA. *Mutat. Res. Mol. Mech. Mutagen.*, **215**, 131–138.
43. Wang, R.Y.H., Kuo, K.C., Gehrke, C.W., Huang, L.-H. and Ehrlich, M. (1982) Heat and alkali-induced deamination of 5-methylcytosine and cytosine residues in DNA. *Biochim. Biophys. Acta*, **697**, 371–377.
44. Shen, J.-C., Rideout, W.M. and Jones, P.A. (1994) The rate of hydrolytic deamination of 5-methylcytosine in double-stranded DNA. *Nucleic Acids Res.*, **22**, 972–976.
45. Zhang, X. and Mathews, C.K. (1994) Effect of DNA cytosine methylation upon deamination-induced mutagenesis in a natural target sequence in duplex DNA. *J. Biol. Chem.*, **269**, 7066–7069.
46. van Loon, B., Markkanen, E. and Hübscher, U. (2010) Oxygen as a friend and enemy: how to combat the mutational potential of 8-oxo-guanine. *DNA Repair (Amst.)*, **9**, 604–616.
47. Obtulowicz, T., Swoboda, M., Speina, E., Gackowski, D., Rozalski, R., Siomek, A., Janik, J., Janowska, B., Cieśla, J.M., Jawien, A. et al. (2010) Oxidative stress and 8-oxoguanine repair are enhanced in colon adenoma and carcinoma patients. *Mutagenesis*, **25**, 463–471.
48. Yu, Y., Cui, Y., Niedernhofer, L.J. and Wang, Y. (2016) Occurrence, biological consequences, and human health relevance of oxidative stress-induced DNA damage. *Chem. Res. Toxicol.*, **29**, 2008–2039.
49. Viel, A., Bruselles, A., Meccia, E., Fornasarig, M., Quaia, M., Canzonieri, V., Policicchio, E., Urso, E.D., Agostini, M., Genuardi, M. et al. (2017) A specific mutational signature associated with DNA 8-Oxoguanine persistence in MUTYH-defective colorectal cancer. *EBioMedicine*, **20**, 39–49.
50. Tate, J.G., Bamford, S., Jubb, H.C., Sondka, Z., Beare, D.M., Bindal, N., Boutselakis, H., Cole, C.G., Creatore, C., Dawson, E. et al. (2019) COSMIC: the catalogue of somatic mutations in cancer. *Nucleic Acids Res.*, **47**, D941–D947.
51. Bouaou, L., Sonkin, D., Ardin, M., Hollstein, M., Byrnes, G., Zavadil, J. and Olivier, M. (2016) TP53 variations in human cancers: new lessons from the IARC TP53 database and genomics data. *Hum. Mutat.*, **37**, 865–876.
52. Schuermann, D., Scheidegger, S.P., Weber, A.R., Björås, M., Leumann, C.J. and Schär, P. (2016) 3CAPS -A structural AP-site analogue as a tool to investigate DNA base excision repair. *Nucleic Acids Res.*, **44**, 2187–2198.
53. Hendrich, B. and Bird, A. (1998) Identification and characterization of a family of mammalian Methyl-CpG binding proteins. *Mol. Cell Biol.*, **18**, 6538–6547.
54. Hsu, C.W., Sowers, M.L., Baljinnam, T., Herring, J.L., Hackfeld, L.C., Tang, H., Zhang, K. and Sowers, L.C. (2022) Measurement of deaminated cytosine adducts in DNA using a novel hybrid thymine DNA glycosylase. *J. Biol. Chem.*, **298**, 101638.
55. Chen, Z. and Ruffner, D.E. (1996) Modified crush-and-soak method for recovering oligodeoxynucleotides from polyacrylamide gel. *BioTechniques*, **21**, 820–822.
56. Kibbe, W.A. (2007) OligoCalc: an online oligonucleotide properties calculator. *Nucleic Acids Res.*, **35**, 43–46.
57. Hosfield, D.J., Frank, G., Weng, Y., Tainer, J.A. and Shen, B. (1998) Newly discovered archaeobacterial flap endonucleases show a structure-specific mechanism for DNA substrate binding and catalysis resembling human flap endonuclease-1. *J. Biol. Chem.*, **273**, 27154–27161.
58. Lin, Y., Beard, W.A., Shock, D.D., Prasad, R., Hou, E.W., Wilson, S.H., Liu, Y., Beard, W.A., Shock, D.D., Prasad, R. et al. (2005) DNA polymerase β and flap endonuclease 1 enzymatic specificities sustain DNA synthesis for long patch base excision repair. *J. Biol. Chem.*, **280**, 3665–3674.
59. Jin, Y.H., Obert, R., Burgers, P.M.J., Kunkel, T.A., Resnick, M.A. and Gordenin, D.A. (2001) The 3'→5' exonuclease of DNA polymerase δ can substitute for the 5' flap endonuclease rad27/fen1 in processing okazaki fragments and preventing genome instability. *Proc. Natl. Acad. Sci. U.S.A.*, **98**, 5122–5127.
60. Shibutani, S., Takeshita, M. and Grollman, A.P. (1991) Insertion of specific bases during DNA synthesis past the oxidation-damaged base 8-oxodG. *Nature*, **349**, 431–434.
61. Petronzelli, F., Riccio, A., Markham, G.D., Seeholzer, S.H., Stoerker, J., Genuardi, M., Yeung, A.T., Matsumoto, Y. and Bellacosa, A. (2000)

- Biphasic kinetics of the human DNA repair protein MED1 (MBD4), a mismatch-specific DNA N-glycosylase. *J. Biol. Chem.*, **275**, 32422–32429.
62. Hendrich, B., Hardeland, U., Ng, H.H., Jiricny, J. and Bird, A. (1999) The thymine glycosylase MBD4 can bind to the product of deamination at methylated CpG sites (Nature (1999) 401 (301-304)). *Nature*, **401**, 301–304.
63. Wu, P., Qiu, C., Sohail, A., Zhang, X., Bhagwat, A.S. and Cheng, X. (2003) Mismatch repair in methylated DNA: structure and activity of the mismatch-specific thymine glycosylase domain of methyl-CpG-binding protein MBD4. *J. Biol. Chem.*, **278**, 5285–5291.
64. Valinluck, V., Liu, P., Kang, J.I. Jr, Burdzy, A., Sowers, L.C., Kang, J.I., Burdzy, A. and Sowers, L.C. (2005) 5-Halogenated pyrimidine lesions within a CpG sequence context mimic 5-methylcytosine by enhancing the binding of the methyl-CpG-binding domain of methyl-CpG-binding protein 2 (MeCP2). *Nucleic Acids Res.*, **33**, 3057–3064.
65. Turner, D.P., Cortellino, S., Schupp, J.E., Caretti, E., Loh, T., Kinsella, T.J. and Bellacosa, A. (2006) The DNA N-glycosylase MED1 exhibits preference for halogenated pyrimidines and is involved in the cytotoxicity of 5-iododeoxyuridine. *Cancer Res.*, **66**, 7686–7693.
66. Schmutte, C., Yang, A.S., Beart, R.W. and Jones, P.A. (1995) Base excision repair of U:G mismatches at a mutational hotspot in the p53 gene is more efficient than base excision repair of T:G mismatches in extracts of human colon tumors. *Cancer Res.*, **55**, 3742–3746.
67. Waters, T.R. and Swann, P.F. (1998) Kinetics of the action of thymine DNA glycosylase. *J. Biol. Chem.*, **273**, 20007–20014.
68. Nandakumar, J., Nair, P.A. and Shuman, S. (2007) Last stop on the road to repair: structure of *E. coli* DNA ligase bound to nicked DNA-Adenylate. *Mol. Cell*, **26**, 257–271.
69. Jaiswal, A.S. and Narayan, S. (2011) Assembly of the base excision repair complex on abasic DNA and role of adenomatous polyposis coli on its functional activity. *Biochemistry*, **50**, 1901–1909.
70. Aceto, G.M., Catalano, T., Curia, M.C. and Tong, Q. (2020) Molecular aspects of colorectal adenomas: the interplay among microenvironment, oxidative stress, and predisposition. *Biomed Res. Int.*, **2020**, 1726309.